Natural Gas for Marine Lean-Burn Spark Ignition Engines
A Combustion Stability Analysis

Kiouranakis, Konstantinos I.; de Vos, Peter; Sapra, Harsh Darshan; Geertsma, Rinze

DOI
10.1115/ICEF2024-139218

Publication date
2024

Document Version
Final published version

Published in
Proceedings of ASME 2024 ICE Forward Conference, ICEF 2024

Proceedings of the ASME 2024
ICE Forward Conference
ICEF2024
October 20-23, 2024, San Antonio, Texas

ICEF2024-139218

NATURAL GAS FOR MARINE LEAN-BURN SPARK IGNITION ENGINES: A COMBUSTION STABILITY ANALYSIS

Konstantinos I. Kiouranakis[1,*], Peter de Vos[1], Harsh Darshan Sapra[2], Rinze Geertsma[1,3]

[1]Faculty of Mechanical Engineering, Delft University of Technology, Netherlands
[2]Department of Mechanical Engineering, University of Wisconsin, U.S.A.
[3]Faculty of Military Sciences, Netherlands Defence Academy, Netherlands

ABSTRACT

Spark-ignition (SI) engines emerge as a viable solution for specific marine applications, offering low-noise operation and emissions mitigation, as well as great potential to utilize high-octane number alternative fuels, such as methanol, ammonia, and hydrogen. However, heavy-duty (HD) SI engines still face challenges such as knocking and combustion instability. Particularly for lean combustion conditions, these engines exhibit the most pronounced cyclic combustion variations. This paper investigates the combustion stability of a 500 kW marine lean-burn natural-gas (NG) engine, a promising candidate for reducing emissions in marine applications. We focus on analyzing in-cylinder pressure measurements to quantify combustion characteristics, emphasizing cycle-to-cycle combustion variation, and exploring the influence of operating parameters like spark timing (ST) and air excess ratio (λ). Our findings demonstrate a clear trade-off between NO_x and COV_{IMEP} emissions through variations in the λ and ST. We identified a transition zone characterized by an increasing number of late-burning cycles at higher λ, before partial burning cycles began at further dilution. Following this, we established a new threshold of 6% for COV_{IMEP} to determine unstable combustion. Notably, increasing dilution from a λ of 1.12 to 1.61 decreased NO_x emissions from 17.83 g/kWh to 0.16 g/kWh, well below IMO Tier III standards, while COV_{IMEP} increased from 1.72% to 13.42%. These insights highlight the potential for advancing SI technology for marine applications and the need for further research to optimize both combustion and emissions in such engines.

Keywords: Internal combustion engine (ICE), marine engineering, maritime, natural gas (NG), alternative fuels, energy transition

NOMENCLATURE

Greek letters

λ	Air excess ratio [-]

Abbreviations

BTE	Brake Thermal Efficiency
CA	Crank Angle
CCV	Cyclic Combustion Variation
CD	Cdombustion Duration
COV	Coefficient Of Variation
CA50	Combustion Phasing
CI	Compression Ignition
CO	Carbon Monoxide
HD	Heavy-Duty
GHRR	Gross Heat Release Rate
ICE	Internal Combustion Engine
IMEP	Indicated Mean Effective Pressure
MFB	Mass Fraction Burnt
NO_x	Nitrogen Oxide
Pmax	Peak Pressure
SI	Spark Ignition
ST	Spark Timing
SO_x	Sulphur Oxide
NG	Natural Gas
UHC	Unburned Hydrocarbons

1. INTRODUCTION

Reciprocating internal combustion engines (ICEs) have long been the foundation of power generation in the marine sector [1], with diesel engines being particularly favored for their high-efficiency and operating robustness [2]. However, despite diesel engine's dominance, spark-ignition (SI) engines emerge as a viable alternative for specific marine applications, such as inland shipping [3]. These engines not only can offer advantages including lower capital costs and reduced noise levels [4], but also the capability to independently operate on high octane renewable fuels like methanol, ammonia, and hydrogen as single fuels [5].

*Corresponding author: K.I.Kiouranakis@tudelft.nl
Documentation for `asmeconf.cls`: Version 1.34, July 6, 2024.

The adoption of natural gas (NG) as a marine engine fuel has notably increased, driven by the efforts of shipping to comply with International Maritime Organization (IMO) regulations like NO_x and SOx [6]. NG is an ideal fuel for the SI technology because of its high octane rating, while it offers short-term advantages over the emerging renewable marine fuels such as existing production capacities and non-toxicity. To this end, marine gas engines will continue playing a crucial role in the maritime industry's endeavors to reduce its environmental impact. Moreover, a better understanding of the performance of heavy-duty (HD) SI natural gas engines can provide valuable insight into performance of such engines on emerging sustainable fuels such as methanol and hydrogen. [5].

High cycle-to-cycle variations and knocking present significant efficiency and power limitations for HD-SI engines [7]. While a common strategy to mitigate knocking and enhance emission performance of these engine is to dilute the mixture, it comes in the expense of exacerbating combustion behavior to a point of very low efficiency levels and elevated emissions of unburned hydrocarbons (UHC) [8]. Slower flame speeds due to dilution, along with greater flame travel distances in larger bores of HD engines, significantly narrows the engine's stable operating range [9–11].

These limitations are particularly pronounced in simpler open-chamber SI engine designs [12, 13], leading to a shift in research towards more sophisticated engine configurations, such as pre-chamber SI and premixed dual-fuel compression ignition (CI) technologies for HD applications. This shift, therefore, has resulted in scarce information regarding the performance and potential enhancements of open-chamber SI engine technology, especially for marine applications [14]. Nevertheless, the relevance of this technology for marine applications is increasingly significant given the urgency to utilize emerging renewable marine fuels, such as methanol and hydrogen.

This paper aims to narrow this gap by investigating the combustion stability of the open chamber SI concept in HD applications. Through an experimental analysis on a 500 kW marine lean-burn NG SI engine, we undertake a detailed examination of in-cylinder pressure measurements from multiple consecutive cycles to assess key combustion and performance characteristics and their cycle-to-cycle variations. Additionally, this study delves into the influence of various operating parameters, such as spark timing (ST) and air excess ratio (λ), on the engine's combustion stability. In this research, we aim to explore pathways for optimizing the performance of HD SI engines and to better understand the combustion stability operating regions for these engines. Our findings could offer valuable insights into alternative ICE technologies for marine applications, showcasing the potential and the challenges of integrating emerging renewable fuels through SI engine concepts.

2. EXPERIMENTAL APPARATUS AND METHODS

2.1 Test engine and data acquisition system

The experiments were conducted with an 8-cylinder, four-stroke, turbocharged marine high-speed NG SI engine, located at the engine laboratory of the Netherlands Defense Academy in Den Helder, as shown in Fig. 1. This engine has a rated power of 500 kW at 1500 rpm, features a minor valve overlap, and powers a directly connected generator at constant speed. Originally designed as a CI engine with a flat cylinder head and a bowl-shaped piston, it was later converted to an SI engine with the injectors replaced by centrally mounted spark plugs. Table 1 lists the main specifications of the tested engine.

FIGURE 1: IMAGE OF THE MARINE FOUR-STROKE SPARK IGNITION ENGINE IN LAB

In the experimental configuration, NG is injected into the engine before the compressor, with its flow rate quantified by a Bronkhorst F-106CI gas flow meter. Note that the NG used in this study is supplied by the central Dutch grid and characterized by its low calorific value. An analysis was conducted to determine the composition and properties of the used NG, with some results summarized in Table 2.

Parameter	Value	Unit
Cylinder number	8	-
Bore x Stroke	170 x 190	mm
Geometric Compression Ratio	12:1	-
Rated Speed	1500	rpm
Rated Power	500	kW
Intake valve open	332.5	°CA aTDC
Intake valve close	-140.0	°CA aTDC
Exhaust valve open	140.0	°CA aTDC
Exhaust valve close	362.5	°CA aTDC

TABLE 1: EXPERIMENTAL ENGINE SPECIFICATIONS

The data acquisition system used in this study is divided in two components: one for in-cylinder measurements, facilitated by a Kistler Kibox, and another designed for external cylinder data collection. This setup incorporates several sensors, including thermocouples and piezoresistive pressure sensors, to measure important mean engine performance parameters such as intake and exhaust pressure and temperature. Emissions analysis, including measurements of NO_x and CO, is conducted using a Horiba PG-350 gas analyzer. Figure 2 provides a schematic of

TABLE 2: NATURAL GAS PROPERTIES

Property	Value	Unit
Methane (CH_4)	80.8	(Vol. %)
Ethane (C_2H_6)	3.18	(Vol. %)
Propane (C_3H_8)	0.71	(Vol. %)
Nitrogen (N_2)	13.1	(Vol. %)
Carbon Dioxide (CO_2)	1.69	(Vol. %)
Density at 25 °C	0.85	kg/m3
Lower calorific value (LCV_{NG})	38.12	MJ/kg

the engine, depicting the placement of the various sensors within this setup. All cylinders are equipped with uncooled Kistler 7061C piezoelectric pressure sensors, connected to a Kistler 5064C charge amplifier. Additionally, an optical crank angle encoder with 720 marks is used to measure the crankshaft angle, enabling pressure data collection with a resolution of 0.5 °CA.

2.2 Operating test method and conditions

All experimental data were collected for steady-state engine operating conditions. To ensure stabilization, the engine was allowed to run for at least ten minutes for each transition between operating points, with continuous online monitoring of several parameters such as exhaust temperature and emissions, to determine whether additional time was required. The experimental study encompassed tests at 18 distinct operating points, including load sweeps from 100 to 450 kW. Following this, sweeps of equivalence ratio and ST were performed at a fixed load of 200 kW, selected for its stability and suitability for the chosen parametric sweeps. For this study, the pressure measurements of cylinder 1, 3, 5, and 7 were captured for 600 consecutive cycles at each measuring operating point.

The engine is equipped with two principal control loops: one maintains constant speed via throttle valve adjustments, and the other maintains the air excess ratio based on a tabulated map by NG entry valve adjustments. These tabulated maps are typically used to comply with NO_x regulations, but in this study are varied to explore the effect of the λ and ST on combustion stability and emissions. It should be noted that the engine's maximum load capability was restricted at 450 kW during these experiments, since attempts to increase the load beyond resulted in the inability of the engine to control its speed. This might be attributed to the open-loop configuration used in this study. Table 3 illustrates the engine test conditions during this experiment.

2.3 Data processing

This engine, previously used in studies [15–17], underwent a detailed analysis to mount new pressure sensors on the cylinder heads [18]. Following this analysis, the new transducers were placed at the periphery of the cylinder in a recessed fashion [8], as shown in Fig. 2. To verify measurement setup's accuracy and ensure the integrity of data used in combustion analysis, offline evaluation techniques were employed [19–21]. The pressure traces were referenced, i.e., pegged, using the two-point polytropic index method [22], automatically implemented within the Kibox for each individual cycle [23]. Filtering was also performed by applying low-pass filter with a cut-off frequency of

TABLE 3: ENGINE TEST CONDITIONS

Sweep	Case	Gen. Power [kW]	NG flow [kg/s]	Air Excess Ratio λ [-]	Spark Timing ST [°CA aTDC]
Load	1	100	0.015	1.17	-20
	2	200	0.023	1.39	-20
	3	300	0.030	1.46	-20
	4	400	0.038	1.47	-20
	5	450	0.042	1.47	-20
Equivalence Ratio	6	200	0.022	1.12	-20
	7	200	0.023	1.26	-20
	8	200	0.023	1.30	-20
	9	200	0.023	1.34	-20
	10	200	0.023	1.46	-20
	11	200	0.025	1.53	-20
	12	200	0.026	1.57	-20
	13	200	0.028	1.61	-20
Spark Timing	14	200	0.024	1.42	-16
	15	200	0.024	1.42	-18
	16	200	0.023	1.43	-22
	17	200	0.022	1.39	-24
	18	200	0.022	1.40	-26

20 kHz. The thermodynamic method of Sta s' [24] was used to determine the thermodynamic loss angle.

Models for performance, stability analysis, and the combustion diagnosis based on the pressure measurements were developed in MATLAB Simulink. The employed heat release model, based on the study of Ding [25], is a zero-dimensional one-zone thermodynamic model adhering to the first law of thermodynamics for a closed system during the non-flow period (inlet valve closing to exhaust valve opening) [7]. An example of its calculations is Eq. 1 that calculates the gross heat release rate. Both crevice and blow-by losses are neglected.

$$GHRR = \dot{Q}_{\text{comb}} = mc_v \frac{dT}{d\theta} + \dot{Q}_{\text{loss}} + p\frac{dV}{d\theta} \tag{1}$$

The mean in-cylinder gas temperature is calculated using the ideal gas equation, treating the in-cylinder mixture of air, fuel, and stoichiometric gases as an ideal yet non-perfect homogeneously mixed gas [26], as shown in Eq. 2. Thermodynamic properties, such as specific heat ratios, depend on the in-cylinder gas' dynamic composition and temperature, calculated for each constituent gas via power series [27, 28].

$$T = \frac{p \cdot V}{m \cdot R} \tag{2}$$

Heat transfer is modeled using the Woschni model to estimate the convective heat transfer coefficient h_{woschni} [29], with the heat loss deriving from Eq. 3.

$$\dot{Q}_{\text{loss}} = A_{\text{wall}} \cdot h_{\text{woschni}} \cdot (T - T_{\text{wall}}) \tag{3}$$

Cycle-to-cycle variations are analyzed through the coefficient of variation (COV) for parameters such as indicated mean effective pressure (IMEP) and peak pressure (P_{max}), defined by Eq. 4, while mean value and standard deviation are given by Eq. 5 and Eq. 6, respectively.

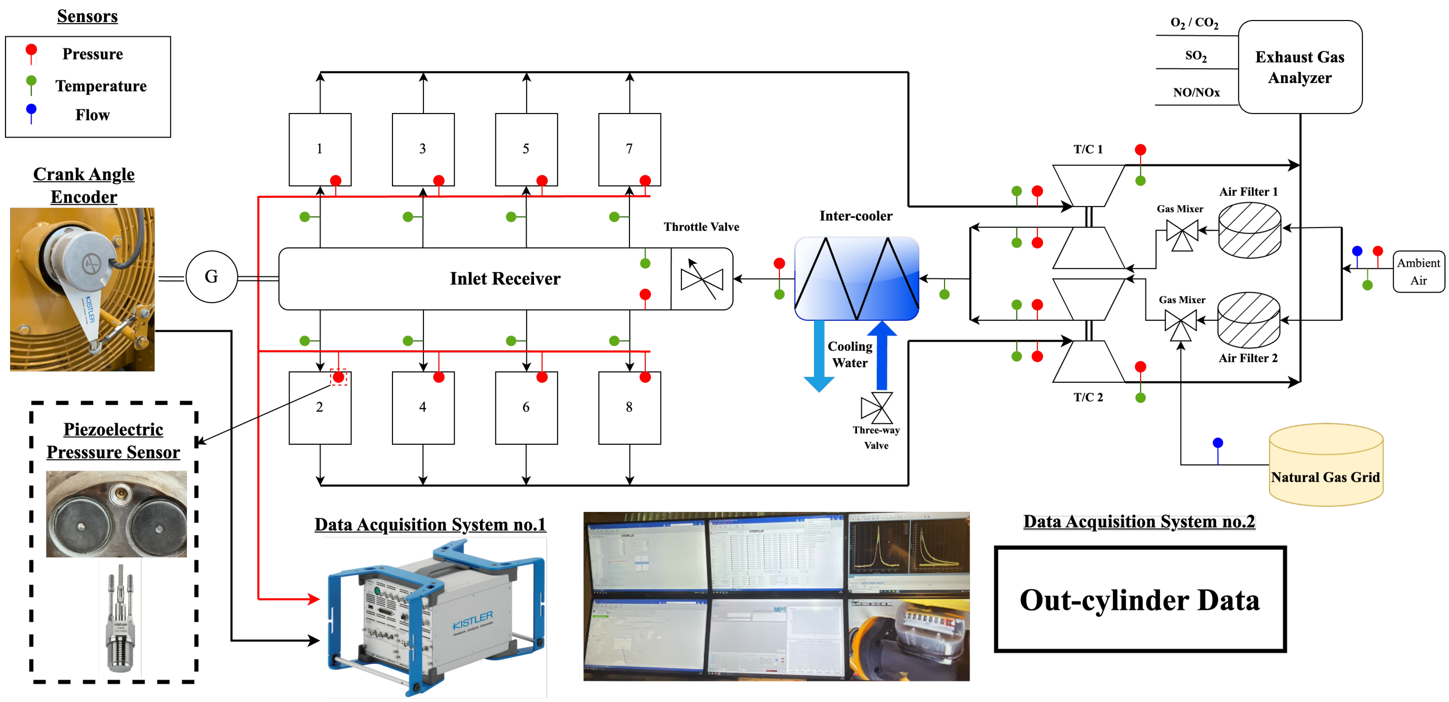

FIGURE 2: SCHEMATIC DIAGRAM OF THE EXPERIMENTAL APPARATUS

$$\mathrm{COV}_x = \frac{\sigma_x}{\mu_x} \cdot 100\% \tag{4}$$

$$\mu_x = \frac{\sum_{i=1}^{N_{\text{cycles}}} x_i}{N_{\text{cycles}}} \tag{5}$$

$$\sigma_x = \sqrt{\frac{\sum_{i=1}^{N_{\text{cycles}}} (x_i - \mu_x)^2}{N_{\text{cycles}}}} \tag{6}$$

To effectively examine cycle combustion variations, it is necessary to assess fuel burning rates through the combustion diagnostic analysis. In this study, we will investigate several combustion parameters derived from the heat release rate (HRR) model, including combustion phasing (CA50), combustion duration (CD), and peak HRR (HRR_{max}). CA50 is defined as the crank angle at which 50% of the fuel has been consumed, with CD being defined as crank angle duration between the combustion of 10% and 90% of the fuel. Our analysis will focus on studying the COV of these three critical combustion parameters.

Brake thermal efficiency (BTE) is calculated based on the engine brake power ($\dot{P}_{\text{brake}}$) in kW and the mass consumption rates of NG ($\dot{m}_{\text{NG}}$) in kg/s, using Eq. 7.

$$\mathrm{BTE} = \frac{\dot{P}_{\text{brake}}}{\dot{m}_{\text{NG}} \cdot \mathrm{LCV}_{\text{NG}}} \cdot 100\% \tag{7}$$

2.4 Methodology for partial burning recognition

Identifying misfires or cycles with partial burning, as well as better understanding the conditions that influence these occurrences, is crucial for both online and offline diagnostics and the subsequent optimization of engine performance. While cyclic variations are inherent in the operation of ICEs, establishing necessary acceptable limits for these variations is essential. Exceeding these limits can deteriorate engine operation, resulting in low efficiency, increased emissions of UHC, and potentially leading to highly unbalanced engine loading, as well as the risk of strong "rebound" that could damage the engine [30]. Realizing the transition zones between stable operating regime and unstable with many partial burns or even misfires is of paramount importance [31]. This can help us enhance our understanding of the impact of various parameters such as ST and λ, and navigate us in the optimization efforts for the trade-offs among the various emissions like $\mathrm{NO_x}$ and UHC and engine efficiency.

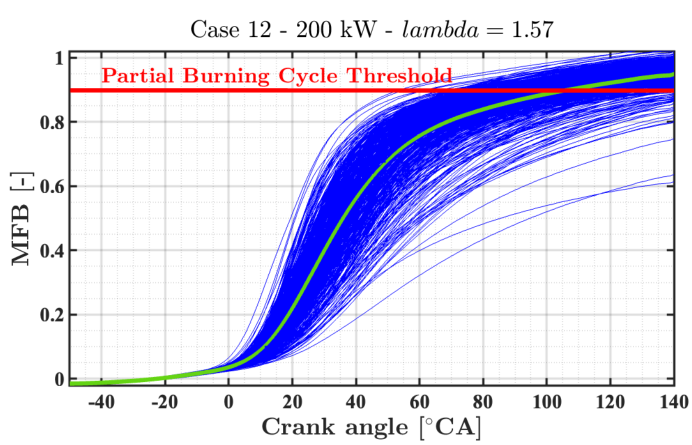

FIGURE 3: PARTIAL BURNING CYCLES IN CASE 12

A misfire cycle is commonly defined as a cycle in which no fuel was combusted, resulting in negative IMEP. On the other hand, consensus on the definitions of partial burning is lacking.

Some studies have set their thresholds for partial burning cycles a less than 50% of the total MFB [32], while others consider cycles with less than 90% [33, 34]. Additionally, the COV [7, 35, 36] and standard deviation [34] of IMEP have also been utilized as an indicator of partial burning by several studies. In this study, individual cycles with total MFB less than 90% at the end of combustion will be considered as partial burning cycles, as found for Case 12 in Fig. 3. By establishing this threshold for individual cycles, we can determine whether a specific operating point is considered unstable [37]. As it will be shown in the subsequent sections, operating points that exhibit at least one individual partial burning cycle out of the cycles measured will be defined as partial burning operating points. For instance, for this engine and the specific measurement setup used, the unstable operating points were identified as test cases 12 and 13, which will be further elaborated upon in subsequent sections.

3. RESULTS AND DISCUSSION

Cyclic combustion variation (CCV) is typically more pronounced in SI engines compared to CI engines [37]. This variability is anticipated in engines operating under lean-burn conditions, especially in those that feature larger bore sizes and open-chamber configurations. Such characteristics lead to weaker flames and longer flame travel distances, making the engine very sensitive to several factors such as local equivalence ratios near the spark plug and residual gases from previous cycles [38].

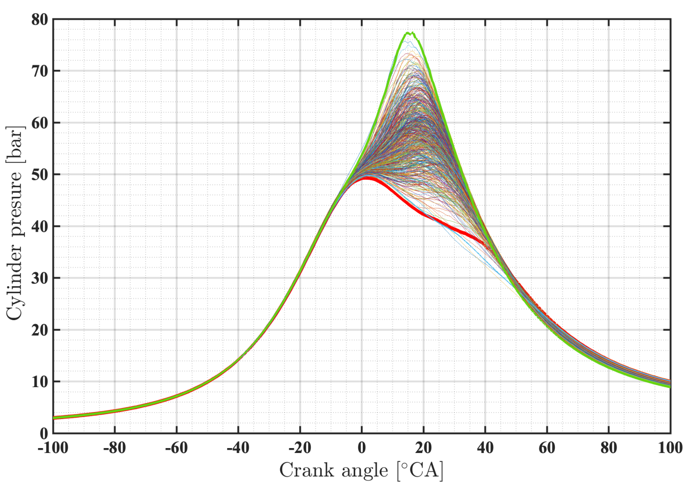

FIGURE 4: PRESSURE-CRANK ANGLE DIAGRAM OF 600 CONSECUTIVE CYCLES IN CASE 4 AND 400 KW LOAD

3.1 Cycle-to-cycle variation

The pressure diagram for cylinder 5 at a load of 400 kW, illustrated in Fig. 4, demonstrates common CCV typically found in SI engines. The pressure traces in green and red color indicate the cycles with the highest and lowest IMEP in the captured 600 cycles, respectively. Note that this engine operates on very lean mixtures at various load points, particularly at higher loads, to comply with NO_x emissions regulations. However, at lower loads — specifically below 200 kW — richer mixtures are employed to prevent poor combustion and potential misfires. The NG used in this experimental setup is characterized by a low calorific value, largely due to its high nitrogen content, as seen in Table 2. Additionally, the engine operates under minor positive valve overlap and its insufficient scavenging efficiency results in retaining some residual gases from one cycle to the following one. This contributes to further dilution of the mixture. Therefore, these factors collectively may account for the observed cycle-to-cycle pressure variations.

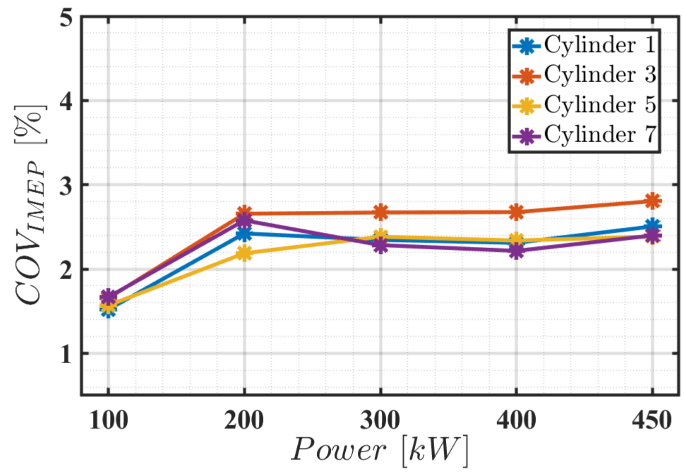

FIGURE 5: COV_{IMEP} FOR ACROSS ALL LOAD POINTS AND CYLINDERS

To better understand CCV along with its impact on engine performance, it is essential to analyze key performance parameters like IMEP across numerous consecutive cycles. Figure 6 illustrates the variations in IMEP, P_{max} and the crank angle of peak pressure occurrence ($CA_{P_{max}}$) at 400 kW. The greatest variability is observed in $CA_{P_{max}}$ for both cycle-to-cycle and cylinder-to-cylinder variations, with COV of 31% for cylinder 5 and range between 26.66% to 35.6% in the four cylinders. Despite this, cycle variations are consistent among all cylinders. The COV_{IMEP} was found 2.33% for cylinder 5 at 400 kW, with a range between 2% and 3% across the cylinders. This variation range among cylinders remained small for all operating points tested, as illustrated in Fig. 5. This consistency in performance parameters like IMEP suggests that cycle-to-cycle variations are significantly more pronounced than cylinder-to-cylinder variations. Consequently, our analysis will predominantly focus on these cycle-to-cycle variations, with cylinder 5 chosen for our investigation to ensure consistency throughout this study.

Figure 7 presents the COV of pressure-related parameters like IMEP and those derived from HRR calculations like CD. Parameters that depend on a single point in the combustion process, such as P_{max}, $CA_{P_{max}}$, HRR_{max}, and CA50, exhibit higher COV values. Conversely, the more holistic parameters of IMEP, which broadly reflects the closed in-cylinder cycle, demonstrates the lowest levels of COV. The COV of $CA_{P_{max}}$ appears to be the most sensitive among all assessed parameters.

The $COV_{HRR_{max}}$ rises with the increasing load, likely due to more intense combustion at higher loads. The lowest values of COV for both CD and CA50 are observed at the highest load of 450 kW, indicating a more consistent combustion at higher

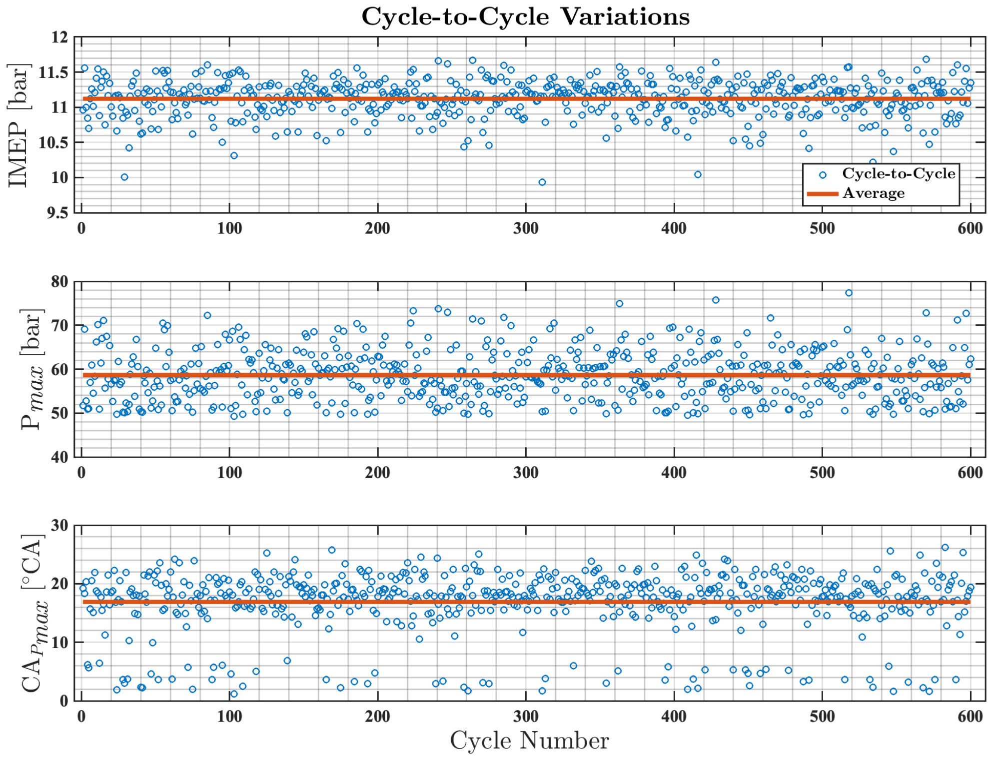

FIGURE 6: CYCLE-TO-CYCLE VARIATION OF PRESSURE-RELATED PARAMETERS AT 400 KW LOAD

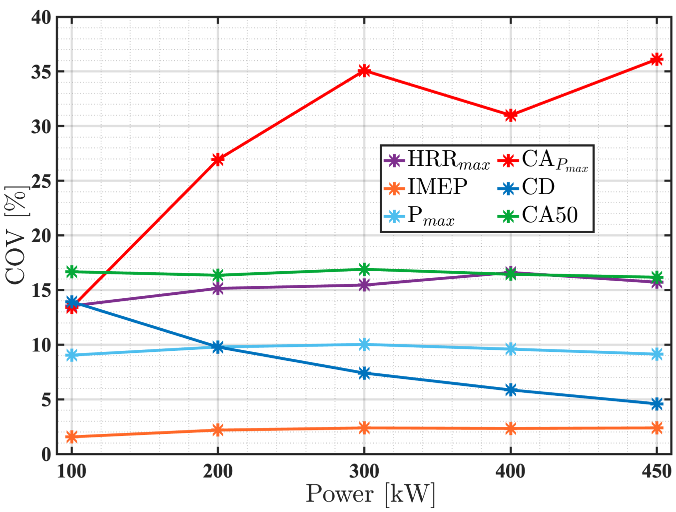

FIGURE 7: COV FOR COMBUSTION AND PERFORMANCE PARAMETERS ACROSS ALL LOAD POINTS

loads due to higher temperatures. Notably, the medium load of 300kW shows slightly higher COV_{CA50} at 16.9% compared to 16.6% at the lowest load of 100 kW, contradicting the expected trend of decreasing COV with increased load, as it also appears in CD. This is likely due to the use of richer mixtures at the lower load point, which shows that the dilution level used in this range outweighed the load effect. However, CA50 variation is relatively consistent in the whole operating load range.

Figure 8a shows the pressure traces at the power of 400 kW, and Fig. 8b depicts the corresponding variations in mass fraction burnt (MFB) for the same operating point. Cycle in red color indicate the cycles that exhibit the lowest levels of IMEP. Although these cycles might be initially considered as partial burning cycles, especially when looking at Fig. 8a, they are instead characterized by significantly delayed combustion phasing that leads to reduced work output [39]. Consequently, these cycles will be characterized as late burning cycles, since they do not lead to total MFB below 90% after the end of combustion, as we defined partial burning cycles as cycles with MFB below 90% in Sec. 2.4. An increasing frequency of these late-burning cycles in an operating point can deteriorate engine efficiency, BTE, and significantly increase CO and UHC emissions due to lower combustion temperatures. Obviously, these increased emission can be confirmed by analysing UHC in exhaust gasses, which is proposed for future work.

3.2 Recognition of combustion stability zones

This study explored several methodologies to define partial burning cycles, as discussed in Sec. 2.4. Our approach has been to utilize either the COV or σ as metrics to assess parameters related to combustion stability. Since COV is directly proportional to σ, as per Eq. 4, correlation is expected between these parameters, as shown by the impact of λ on both parameters for IMEP in Fig. 17 of the Appendix. Consequently, COV is selected over σ in this study, because of the ability of COV as a parameter to effectively compare the degree of variation among data series of different

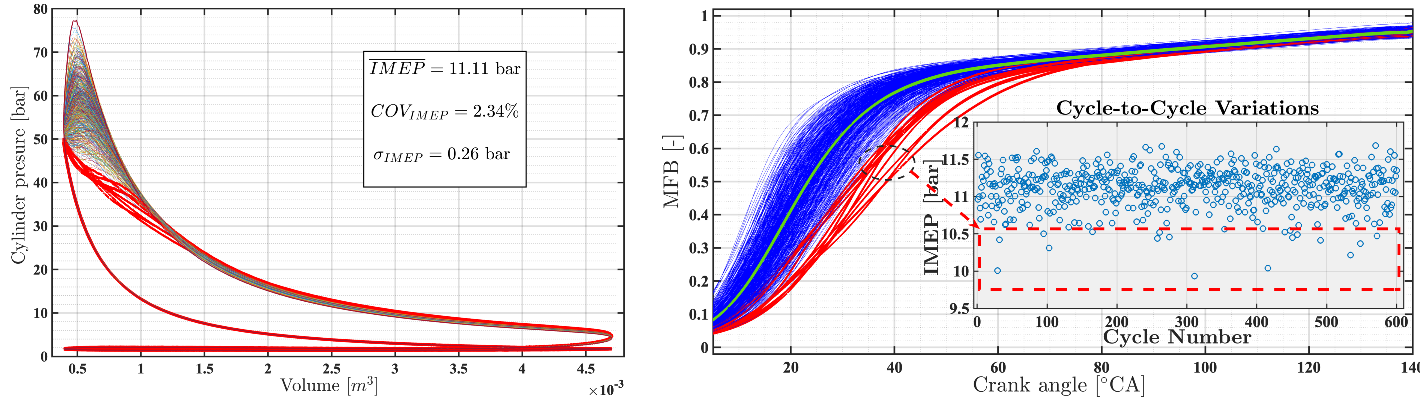

(a) Pressure-Volume diagram

(b) Mass fraction burnt variation

FIGURE 8: VISUALIZATION OF LATE BURNING CYCLES AT 400 KW LOAD

scale. More specifically, COV_{IMEP} has been selected as the metric for assessing combustion stability. The selection of IMEP over other parameters was influenced by several considerations:

- Simplicity: IMEP does not require HRR calculations, making it a straightforward choice.
- Consistency: P_{max} variations were found relatively inconsistent when higher CCV were observed. For instance, during the λ sweep, opposite trends were identified between the COV of P_{max} and that of IMEP and $CA_{P_{max}}$, as shown in Fig. 18 of the Appendix.
- Holistic assessment: IMEP provides a holistic view of the closed cycle, thereby preferred over $CA_{P_{max}}$.

In Sec. 3.1, late burning cycles, rather than partial burning, were identified as the main contributors to IMEP variation due to very late burning. An increasing number of these late burning cycles at an operation point could be characterized as the precursor to a partial burning operation that would take place, for instance, in case of further dilution. This occurs since the combustion extends so far into the expansion phase that temperatures are lower and a significant portion of fuel cannot be burned, leading to decreased combustion efficiency. The tendency of these late-burning cycles is effectively captured by the increase in COV_{IMEP}. This correlation is further supported by the relationship between COV_{IMEP} and COV of combustion phasing parameters like CA50, which are typically sensitive to late-burning. Further analysis across all tested operating points demonstrated that COV_{IMEP} maintains high correlation with several combustion phasing parameters such as CA70, CA75, and CA80, defined by the percentage of total fuel consumed. These correlations were found with R^2 ranging from 0.87 to 0.91, with CA75 exhibiting the highest, as illustrated in Fig. 19 of the Appendix. This strong correlation, together with variations observed in MFB, e.g., the ones illustrated in Fig. 8b, suggests that late combustion phasing parameters like CA75 may be more effective indicators of late burning compared to CA50.

To define the combustion stability zones of an engine, it is crucial to better understand the impact of combustion variation on its performance. Figure 9 demonstrates how dilution affects both BTE and COV_{IMEP}, revealing a clear inverse trend between these parameters as dilution increases. Note that the λ sweep was used to determine the stability zones, since the extent of ST delay tested in this experimental study did not appear to deteriorate CCV to the same extent as λ, as illustrated in Fig. 20 of the Appendix. The insights gained from the impact of dilution on CCV, and its subsequent effect on BTE and CO, as shown in Fig. 10, have led to the establishment of a threshold for COV_{IMEP}. It should be noted that there are two distinct outliers in the trend of both NO_x and CO, the measurement for Case 7 at λ of 1.26. These measurements can be deemed as unreliable due to challenges with the emission measurement system encountered during its capturing.

Three main combustion stability regions are defined:

1. **Stable Combustion Zone:** Characterized by very low levels of COV_{IMEP} and high levels of BTE, indicating an efficient engine operation.
2. **Transition Zone:** Marked by an increase in late-burning cycles, suggesting the onset of combustion instability.
3. **Unstable Combustion Zone:** Defined by the occurrence of partial-burning cycles, which significantly deteriorate efficiency and stability.

The transition from λ of 1.39 to λ of 1.46 led to the first shift towards the transition zone, where the occurrence of partial burning cycles started increasing. However, the transition from λ of 1.53 to λ of 1.57 resulted in a critical shift, with a further increase in the slopes for both BTE and COV_{IMEP}. This is also confirmed by similar rise in the slope of CO emissions with the further dilution. This shift occurs at COV_{IMEP} of 5.32%, and it is corroborated by the appearance of partial burning cycles in Case 12 with λ of 1.57, as illustrated in Fig. 3. Further, partial burning cycles exhibit greater impact on the COV_{IMEP} than late burning cycles. Based on these observations, we propose a threshold COV_{IMEP} of 6% to characterize unstable combustion, as this is approximately where partial burning starts to occur. This threshold can potentially be applied to other similar HD-SI engines to assist in identifying unstable combustion conditions.

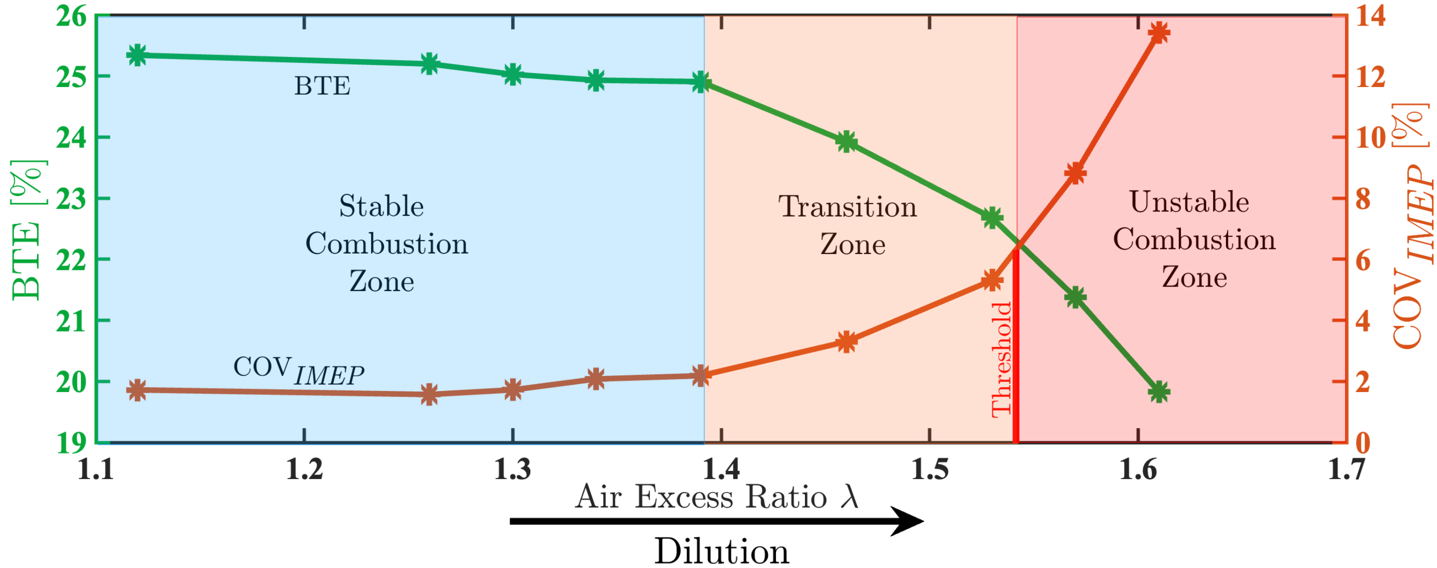

FIGURE 9: IDENTIFICATION OF COMBUSTION STABILITY ZONES IN ENGINE OPERATION

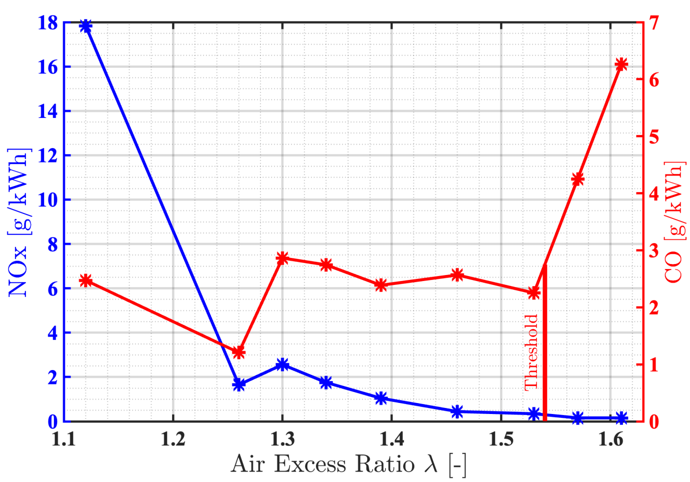

FIGURE 10: IMPACT OF λ VARIATION ON NO_X AND CO EMISSIONS

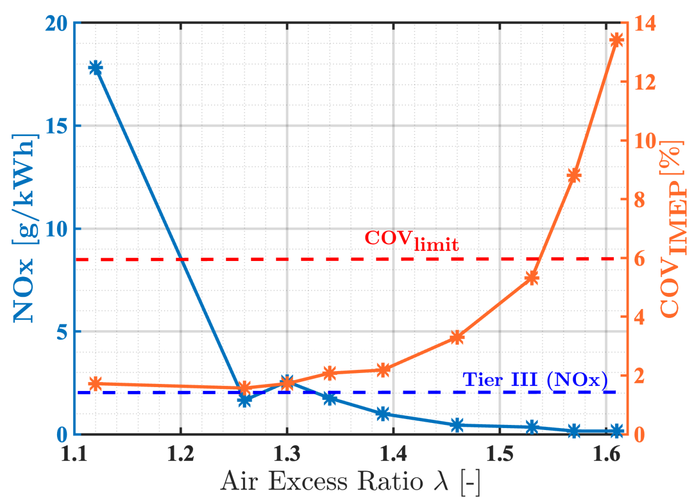

FIGURE 11: IMPACT OF λ VARIATION ON NO_X AND COV_{IMEP}

3.3 Effect of air-fuel ratio

Diluting the mixture through very lean mixtures or exhaust gas recirculation is commonly employed to improve emissions performance, particularly regarding NO_x emissions in SI engines, usually compromising efficiency. However, excessive dilution can deteriorate combustion stability to the extent of significantly lower efficiencies and elevated UHC emissions. Figure 11 illustrates the impact of a leaning sweep on NO_x and COV_{IMEP} at the constant load of 200kW, along with the limits for Tier III NO_x set by IMO and COV set by this study.

At the lowest λ of 1.12, NO_x emissions significantly increased to 17.73 g/kWh, while COV_{IMEP} remained low at 1.72%. Interestingly, leaning the mixture from λ of 1.12 to 1.26 slightly decreased COV_{IMEP} to 1.57%. This reduction in CCV is further evidenced by the distinct decrease in the COV_{CD} for the leaner mixture, as depicted in Fig. 12. The higher CCV observed in the richer mixture can be attributed to an increased frequency of well-burning combustion cycles of greater intensity. Therefore, such cycles introduce a certain degree of variability as the mixture approaches stoichiometric conditions.

Further dilution of the mixture generally leads to higher CCV, with λ values of 1.39 and 1.53 being critical points in this study. At these points, the sensitivity of COV to dilution intensifies, as indicated by the steep increase in slope of COV_{IMEP} in Fig. 11. These points also mark the transitions discussed in Sec. 3.2, where dilution with λ beyond 1.53 exceeds the combustion stability limit.

As demonstrated in Fig. 12, the $COV_{HRR_{max}}$ consistently increases with leaner mixtures, rising from 12.31% to 27.56%. The COV_{CA50} peaked for the two leanest mixtures due to the occurrence of many partial burning cycles. Interestingly, the points of minimum variation for CA50 and CD do not coincide, with the former occurring at λ of 1.39 and the latter at λ of 1.23. This pattern for COV_{CA50} can be attributed to a good balance between

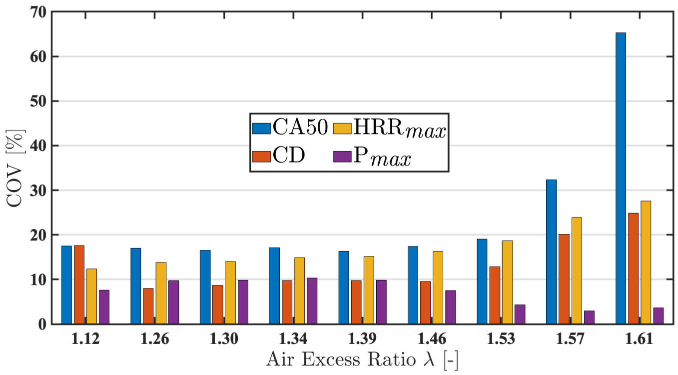

FIGURE 12: COV OF COMBUSTION PARAMETERS ACROSS THE λ SWEEP

intense well-burning cycles and less intense ones, which is not present in richer mixtures. Conversely, faster combustion rates across most cycles at λ of 1.23 results in the minimization of COV_{CD}. Regarding the $COV_{P_{max}}$, it consistently decreases with dilution because combustion is extended so much towards late expansion, resulting in pressures that do not exceed those at TDC.

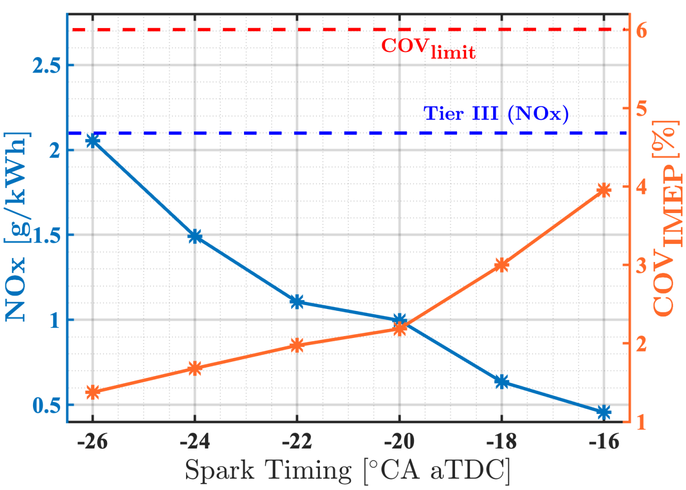

FIGURE 13: IMPACT OF ST VARIATION ON NO_X AND COV_{IMEP}

3.4 Effect of spark timing

ST is another crucial factor that can affect combustion stability and emissions performance of an SI engine. Figure 13 illustrates the effects of ST in NO_x emissions and the COV_{IMEP} at the constant load of 200 kW. Note that at more delayed ST settings, a slight adjustments in λ took place by the engine speed controller compensating for rougher combustion by increasing fuel input. Delaying ST exhibits trends similar to mixture dilution, with a consistent decrease in NO_x and an increase in the COV_{IMEP}. The sensitivity to changes in ST was notably different between the increments from -26 to -20 and from -20 to -16, with increased sensitivity observed in the latter range. This suggests a potential combustion phasing thresholds for this load, from where further ST delay leads to significantly higher levels of cyclic variations.

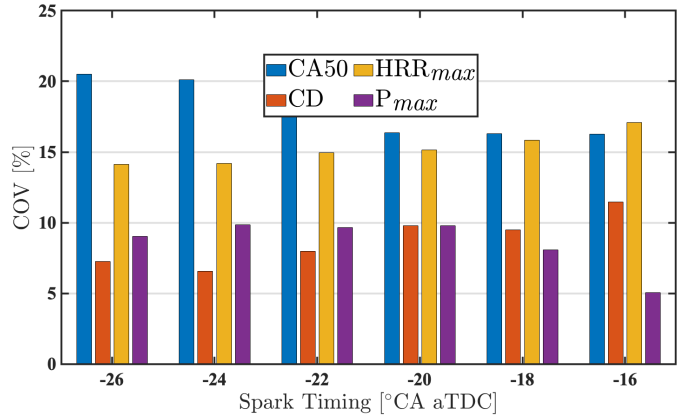

FIGURE 14: COV OF COMBUSTION PARAMETERS ACROSS THE ST SWEEP

The COV_{CA50} demonstrates an opposite trend from COV_{CD} with delaying ST, as illustrated by the Fig. 14. Interestingly, COV_{CA50} reaches its highest values at more advanced ST. This trend contradicts the expected behavior of more stable combustion with more advanced ST, as indicated by COV_{CD} and COV_{IMEP}. This could be due to significantly smaller mean value of CA at advanced combustion stages, closer to TDC. This smaller mean value can exaggerate the COV, masking the real variation. Therefore, in such cases, it might be more reasonable to compare standard deviations rather than COV to avoid misleading interpretations of CCV, as depicted in Fig. 15. Conversely, more advanced ST results in reduced COV_{CD} due to faster combustion rates. However, the minimum COV_{CD} is not observed at the most advanced ST, but rather with ST of -26. This mirrors the findings from the λ sweep, where the second richest mixture led to the minimum COV_{CD}. These observations imply that there are optimal settings for ST and λ that can significantly enhance engine performance at various operating points. Regarding the trends in $COV_{HRR_{max}}$ and $COV_{P_{max}}$ with ST delay, they exhibit the same trends as with mixture dilution.

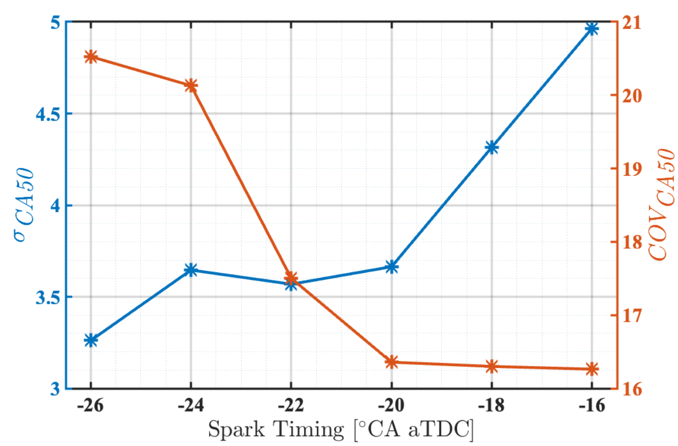

FIGURE 15: IMPACT OF ST DELAY ON COV AND σ OF CA50

Further, none of the operating points resulted in COV_{IMEP} and NO_x that exceeded the limits, highlighting the effectiveness of ST to improve combustion stability without significantly compromising emission performance. However, despite not exceeding the COV_{IMEP} limit, the stability has entered the transition zone with ST delay beyond -20. This can also be confirmed by the exhaust temperatures correlating with COV_{IMEP} with ST adjustments, as illustrated in Fig. 16. Additionally, given the high correlation between exhaust temperature and COV_{CD}, exhaust temperature could be further used as a valuable indicator for monitoring increases in cyclic variations potentially improving online control strategies.

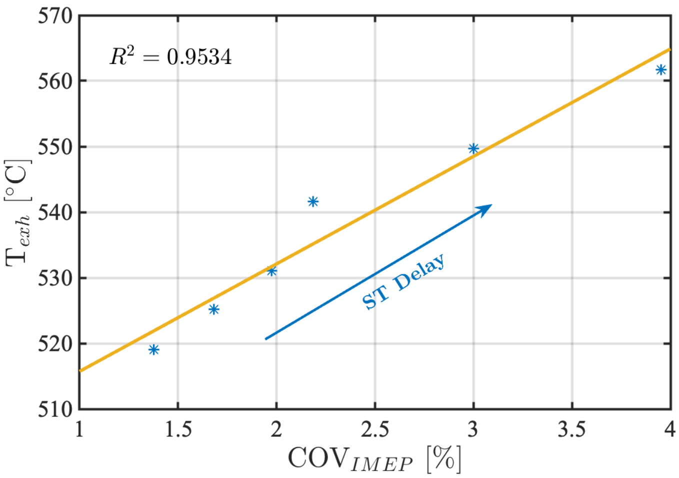

FIGURE 16: IMPACT OF ST DELAY ON T_{EXH} AND COV_{IMEP}

4. CONCLUSIONS AND RECOMMENDATIONS

In this study, we conducted combustion stability analysis in a marine open-chamber SI engine fueled by NG, aiming to understand cyclic combustion variation (CCV), as well as identify the boundaries of stable operating regions and their potential optimization routes. For such engines, a transition zone was identified when the air excess ratio is increased, in which the combustion starts to be significantly delayed, before partial burning occurs after even further dilution. A threshold of 6% for COV_{IMEP} is proposed to characterize unstable operations as this value corresponds approximately to the point at which partial burning cycles with combustion efficiency below 90% start to occur, which might be applicable to similar engines. Adjusting the mixture from λ of 1.12 to 1.61 lowered NO_x emissions from 17.83 g/kWh to 0.16 g/kWh, far below IMO Tier III standards, but at the expense of an increase of COV_{IMEP} from 1.72% to 13.42%. Diluting the mixture beyond λ of 1.53 resulted in unstable combustion with appearance of partial burning cycles. Additionally, both NO_x and COV_{IMEP} exhibited higher sensitivity to dilution compared to ST adjustment explored in this study. All tested ST at 200kW, ranging from -26 to -16, met both NO_x and combustion stability limits.

For future research, exploring the impact of higher calorific NG would be interesting, particularly to determine whether different sensitivity levels emerge for combustion at higher calorific values. Additionally, studying the influence of charge air temperature on the trade-off between combustion stability and emissions would be valuable. Besides NO_x and CO, further studies should also focus on the relationship between the COV_{IMEP} and UHC for these types of premixed engines. Measurements of UHC in these engines, especially methane slip, is vital due to the global warming impact of unburnt methane. This analysis is particularly relevant as these engines, including the specific setup proposed for conversion to 100% methanol, show great potential for running on emerging renewable fuels. Understanding these relationships could provide critical insights into optimizing engine performance and minimizing emissions across these engine concepts fully operated on renewable fuels, enhancing the sustainability of marine propulsion systems.

ACKNOWLEDGMENTS

The present research is a part of the MENENS project (Methanol als Energiestap Naar Emissieloze Nederlandse Scheepvaart). The project is funded by the Netherlands Enterprise Agency (RVO: Rijksdienst voor Ondernemend Nederland). Gratidute is extended to the Netherlands Defence Academy (NLDA) engine lab team for their unwavering support.

REFERENCES

[1] Curran, Scott et al. "The future of ship engines: Renewable fuels and enabling technologies for decarbonization." *International Journal of Engine Research* (2023)DOI 10.1177/14680874231187954.

[2] Kalghatgi, Gautam. "Is it really the end of internal combustion engines and petroleum in transport?" *Applied Energy* Vol. 225 (2018). DOI 10.1016/j.apenergy.2018.05.076.

[3] Kiouranakis, K.I., de Vos, Peter and Geertsma, R.D. "Methanol as a Fuel in Shipping: Review and Outlook to ICE Research within MENENS." *TRA2024*. 2024. Springer, Dublin, Ireland.

[4] Mahendar, Senthil Krishnan and Erlandsson, Anders. "Challenges for Spark Ignition Engines in Heavy Duty Application: a Review." 2018. DOI 10.4271/2018-01-0907.

[5] Downes, Trevor and Auld, Andrew. "A dedicated spark-ignited heavy-duty engine for multiple future fuels." *Heavy-Duty-, On- und Off-Highway-Motoren 2020*. Springer Fachmedien Wiesbaden, Wiesbaden (2021). DOI 10.1007/978-3-658-34362-0_10.

[6] Burel, Fabio, Taccani, Rodolfo and Zuliani, Nicola. "Improving sustainability of maritime transport through utilization of Liquefied Natural Gas (LNG) for propulsion." *Energy* Vol. 57 (2013). DOI 10.1016/j.energy.2013.05.002.

[7] Heywood, John B. *Internal combustion engine fundamentals*, second edition ed. McGraw-Hill Education, New York (2018).

[8] Kumar, Maurya Rakesh, Maurya, Luby and Luby. *Reciprocating Engine Combustion Diagnostics: In-Cylinder Pressure Measurement and Analysis*, 1st ed. Mechanical Engineering Series, Springer (2019). DOI 10.1007/978-3-030-11954-6.

[9] Sapra, Harsh et al. "Hydrogen-natural gas combustion in a marine lean-burn SI engine: A comparitive analysis of Seiliger and double Wiebe function-based zero–dimensional modelling." *Energy Conversion and Management* Vol. 207 (2020). DOI 10.1016/j.enconman.2020.112494.

[10] Issei, Ohashi. "Dual-Fuel Marine Engine (Highly Reliable Environmentally Friendly Engine) Technical Review." Technical report no. YANMAR. 2015. URL https://www.yanmar.com/global/about/technology/technical_review/2015/0727_2.html.

[11] Tavakoli, Sadi et al. "Modeling and analysis of performance and emissions of marine lean-burn natural gas engine propulsion in waves." *Applied Energy* Vol. 279 (2020). DOI 10.1016/j.apenergy.2020.115904.

[12] Humerfelt, T., Johannessen, E., Vaktskjold, E. and Skarbö, L. "Development of The Rolls-Royce C26: 33 Marine Gas Engine Series." *26th CIMAC World Congress*. 2010.

[13] Marquez, Manuel Alejandro Echeverri et al. "A Pathway to Ultra-Lean IC Engine Combustion: The Narrow Throat Pre-chamber." *Engines and Fuels for Future Transport*. Springer (2022).

[14] Krivopolianskii, Vladimir et al. "Control of the combustion process and emission formation in marine gas engines." *Journal of Marine Science and Technology* Vol. 24 (2019). DOI 10.1007/s00773-018-0556-0.

[15] Sapra, Harsh et al. "Experimental Investigations of Hydrogen-Natural Gas Engines for Maritime Applications." *Internal Combustion Engine Division Fall Technical Conference, American Society of Mechanical Engineers*. 2018.

[16] Sapra, Harsh et al. "Experimental investigations of performance variations in marine hydrogen-natural gas engines." *28th CIMAC World Congress*. 2019.

[17] Bosklopper, J. et al. "Experimental study on a retrofitted marine size spark-ignition engine running on portinjected 100% methanol." *INEC 2020, Delft* (2020).

[18] Soltis, Dennis A. "Evaluation of Cylinder Pressure Transducer Accuracy based upon Mounting Style, Heat Shields, and Watercooling." 2005. DOI 10.4271/2005-01-3750.

[19] Lancaster, David R., Krieger, Roger B. and Lienesch, John H. "Measurement and Analysis of Engine Pressure Data." 1975. DOI 10.4271/750026.

[20] Brunt, Michael F. J. and Pond, Christopher R. "Evaluation of Techniques for Absolute Cylinder Pressure Correction." 1997. DOI 10.4271/970036.

[21] Payri, F. et al. "Digital signal processing of in-cylinder pressure for combustion diagnosis of internal combustion engines." *Mechanical Systems and Signal Processing* Vol. 24 (2010). DOI 10.1016/j.ymssp.2009.12.011.

[22] Randolph, Andrew L. "Methods of Processing Cylinder-Pressure Transducer Signals to Maximize Data Accuracy." 1990. DOI 10.4271/900170.

[23] AG, Kistler. "Instruction Manual KiBox To Go Type 2893A." (2018).

[24] Sta S, Marek J. "Thermodynamic Determination of T.D.C. in Piston Combustion Engines." 1996. DOI 10.4271/960610.

[25] Ding, Yu. *Characterising combustion in diesel engines using parameterised finite stage cylinder process models*. Delft (2011).

[26] Stapersma, D. *Diesel engines: A fundamental approach to performance analysis, turbocharging, combustion, emissions and heat transfer : Including thermodynamical principles. Vol. 3: Combustion*. v. 1, TU Delft (2009).

[27] Borman, Gary L. and Ragland, Kenneth W. *Combustion engineering*. McGraw-Hill, Boston (1998).

[28] McBride, Bonnie J. *Coefficients for calculating thermodynamic and transport properties of individual species* (1993).

[29] Woschni, G. "A Universally Applicable Equation for the Instantaneous Heat Transfer Coefficient in the Internal Combustion Engine." 1967. DOI 10.4271/670931.

[30] Finney, Charles Ea et al. "Invited Review: A review of deterministic effects in cyclic variability of internal combustion engines." *International Journal of Engine Research* Vol. 16 (2015). DOI 10.1177/1468087415572033.

[31] Kaul, Brian, et al. "High-dilution stoichiometric gasoline direct-injection (SGDI) combustion control development." (2016).

[32] Peterson, Brian, Reuss, David L. and Sick, Volker. "High-speed imaging analysis of misfires in a spray-guided direct injection engine." *Proceedings of the Combustion Institute* Vol. 33 (2011). DOI 10.1016/j.proci.2010.07.079.

[33] Bahri, Bahram aand others. "Understanding and detecting misfire in an HCCI engine fuelled with ethanol." *Applied Energy* (2013)DOI 10.1016/j.apenergy.2013.03.004.

[34] Sjöberg, Magnus and Dec, John E. "Comparing late-cycle autoignition stability for single- and two-stage ignition fuels in HCCI engines." *Proceedings of the Combustion Institute* Vol. 31 (2007). DOI 10.1016/j.proci.2006.08.010.

[35] Biswas, Srijit et al. "Assessing the potential of ethanol in the transition of biodiesel combustion to RCCI regimes under varying injection phasing strategies: A performance-emission-stability and tribological perspective." *Fuel* Vol. 304 (2021). DOI 10.1016/j.fuel.2021.121346.

[36] Diané, Ali et al. "Characterization, at Partial Loads, of the Combustion and Emissions of a Dual-Fuel Engine Burning Diesel and a Lean Gas Surrogate." *Energies* Vol. 16 (2023). DOI 10.3390/en16155587.

[37] Maurya, Rakesh Kumar. *Characteristics and Control of Low Temperature Combustion Engines*. Mechanical Engineering Series, Springer International Publishing, Cham (2018). DOI 10.1007/978-3-319-68508-3.

[38] Ozdor, Nir et al. "An Experimental Study of the Cyclic Variability in Spark Ignition Engines." 1996. DOI 10.4271/960611.

[39] Erman, Aydek Gökçe, Hellier, Paul and Ladommatos, Nicos. "The impact of ignition delay and further fuel properties on combustion and emissions in a compression ignition engine." *Fuel* (2020)DOI 10.1016/j.fuel.2019.116155.

APPENDIX A. SUPPLEMENTARY FIGURES

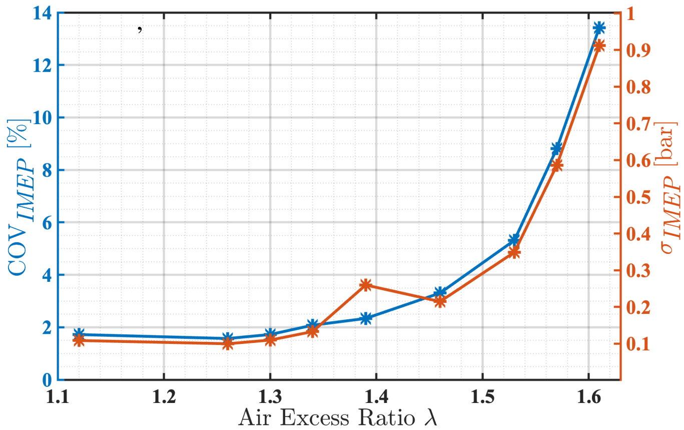

FIGURE 17: IMPACT OF λ VARIATION ON COV AND σ OF IMEP

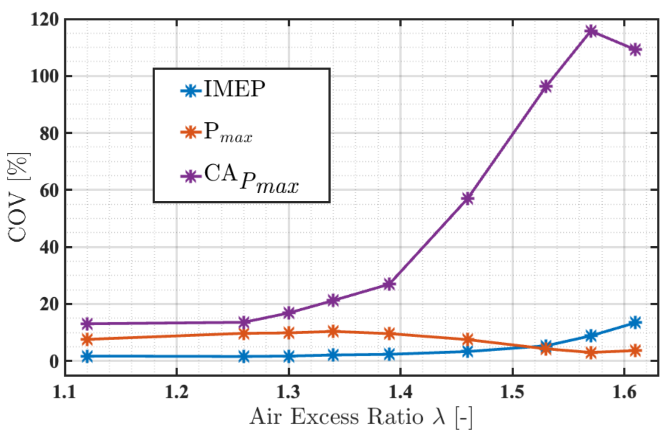

FIGURE 18: COV OF IMEP, P_{max}, AND $CA_{P_{max}}$ FOR THE λ SWEEP

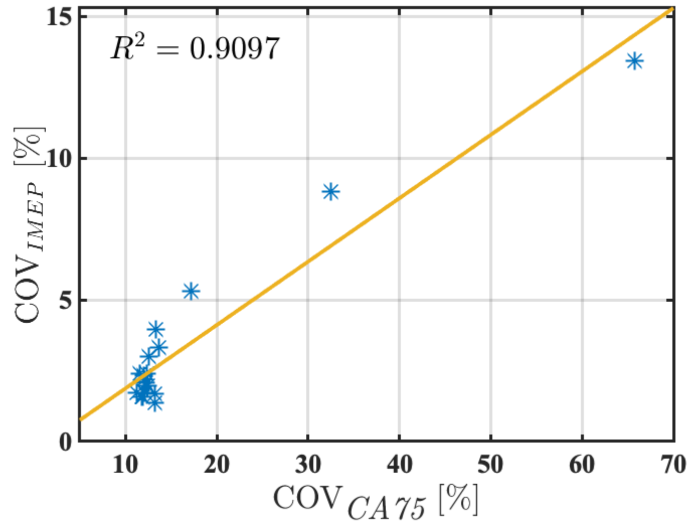

FIGURE 19: CORRELATION BETWEEN COV_{IMEP} AND COV_{CA75}

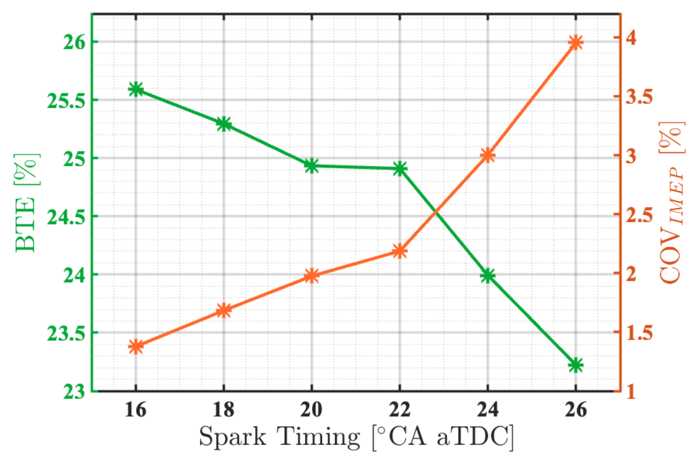

FIGURE 20: IMPACT OF ST ON COV_{IMEP} AND BTE